Volume 4, Issue 4, 2015, 316-320 ISSN 2284-6808

Letters in Applied NanoBioScience

www.NanoBioLetters.com

Original Research Article Open Access Journal

Received: 15.08.2015 / Revised: 20.09.2015 / Accepted: 15.10.2015 / Published on-line: 30.11.2015

High-Resolution Imaging of Cells Using Current Sensing Atomic Force Microscopy

Lifang Shi [1], Allard Katan [2], Jianli Zhao [1], Miquel Salmeron [2,*], Gang-yu Liu [1]**

[1]Department of Chemistry, University of California, Davis, California 95616, USA

[2]Materials Sciences Division, Lawrence Berkeley National Laboratory, University of California, Berkeley, California 94720, USA

*corresponding author e-mail address: ***mbsalmeron@lbl.gov***

corresponding author e-mail address: ***gyliu@ucdavis.edu*

ABSTRACT

This paper introduces a new and simple approach using atomic force microscopy (AFM) for high-resolution cellular imaging. To overcome difficulties to attain nanometer resolution cellular imaging, transition metal ions were introduced to cells, followed by current sensing AFM. In the case of Pt(II) stained NIH3T3 cells, topography and current images reveal the morphology and structural features, such as villi, podia, and fiber assemblies. Finer membrane features (< 20 nm) are also observed. The rational for current contrast is also investigated. The simplicity and high-resolution of this method shall prove helpful, convenient, and informative for researchers pursuing bio-imaging without involving complex instrumentation, protocols, and/or sectioning of samples.

Keywords: *Cellular imaging; Current sensing atomic force microscopy; High-resolution bio-imaging.*

1. INTRODUCTION

Atomic force microscopy (AFM), originally reported by Binnig et al., [1] has been widely used for bio-imaging during the last two decades due to its high resolution, operation in near physiological conditions, and ability to image in real-time to study dynamics [2-7].

In principle, the cellular membrane should be visualized by AFM with high-resolution [8]. However, it has been very challenging to reach nanometer resolution due to the soft-and-sticky interactions between the AFM probe and sample underneath, as well as the high mobility of lipid molecules within membrane [9]. Continuous efforts to address these challenges include advanced imaging modes such as non-contact mode [10-12], and contact resonance imaging [13]; and specialty probes, e.g., carbon-nanotubes [6,14-17].

These approaches have reduced the impact of soft-and-sticky interactions, and have shown improvement in imaging resolution. Other approaches involve significant changes in AFM configuration, e.g. (a) imaging cellular membrane via sensing ionic exchanges through membrane pores [18]; (b) scanning ion conductance microscopy (SICM) imaging, the contrast of which depends on ion current [9,19,20] (c) scanning electrochemical microscopy (SECM) imaging utilizing redox current [18,21-24].

For most researchers using AFM, it would be a technical advantage to be able to visualize cells with high resolution without significant change of the instrument configuration.

This paper reports a new approach of high-resolution imaging of cells by using a current sensing atomic force microscopy (CAFM). CAFM is a common option supported by most AFM instruments to provide topographic images and simultaneous current images [25-28]. For the initial investigation, NIH 3T3 cells were first fixed to preserve structural integrity.

To ensure CAFM contrast, Pt(II) ions were introduced via coordination with intracellular amine residues to enhance conductivity. Characteristic structural features were revealed in the current images with resolution of tens of nanometers.

2. EXPERIMENTAL SECTION

Au(111) substrates were prepared by thermal evaporation of Au (99.999%, Alfa Aesar, MA) in a high vacuum evaporator (Denton Vacuum, Inc., model 502-A) with a base pressure 3 $\times 10^{-7}$Torr during evaporation. 200 nm gold films were deposited onto freshly cleaved mica(0001) surfaces (clear ruby muscovite, Mica New York Corp. NY), at a substrate temperature of 350 °C and a rate of 3 Å/s. Subsequently, the films were annealed in situ at 375 °C for 20 min, cooled to room temperature under vacuum, and subject to hydrogen flaming (99.99%, Praxair Inc. CT) before use. Self-assembled monolayers (SAMs) were prepared following well-known procedures [29-31]. 11-mercapto-1-undecanal disulfide, $[S(CH_2)_{10}CHO]_2$, 99% purity, was purchased from ProChimia (Gdansk, Poland) and used without further treatment. 0.5 mM $[S(CH_2)_{10}CHO]_2$ solutions were prepared in 99.99% purity ethanol (Gold Shield Chemical Co. CA). Freshly prepared Au(111) substrates were immersed into the prepared solutions for 24 h at room temperature. The disulfide bonds dissociate on gold surfaces upon chemisorption, forming SAMs of $CHO(CH_2)_{10}S$/Au(111) [32,33].

Mouse embryonic fibroblast NIH 3T3 cells were used for this investigation, whose culturing followed previously established protocols.[34] Cells were purchased from A.T.C.C (Manassas, VA). The cells were maintained in Dulbecco's modified Eagle's media (DMEM, GIBCO-BRL, Grand Island, NY) supplemented with 10% heat-inactivated fetal bovine serum (HyClone, Logan, UT), penicillin (100 U/ml), and streptomycin (100 g/ml) (GIBCO-BRL,

Grand Island, NY) at 37 °C and 5% CO_2 in a standard incubator (NAPCO SERIES 8000WJ, Thermo Scientific, MA). The sample preparation for CAFM imaging follows the following protocols. First, SAMs were soaked in a 10 μg/ml fibronectin (FN) (Millipore, Temecula, CA) solution for 1hr to essure the protein immobilization. It was known the amine resides in FN attach to aldehyde termini forming imine bonds [35]. Then, NIH 3T3 cells were plated on the FN-functionalized substrates in culture media, and allowed to incubate for 24 hrs to reach healthy status with mature focal adhesion with known spreading and morphology. Upon taking the sample out of incubation, cells were fixed using a standard 3.7% formaldehyde solution for 1 hr at room temperature. The fixation solution was then removed, followed by adding an aqueous solution containing 10 $\mu M K_2PtCl_4$ (99.99 %, Alfa Aesar, MA)at a molar ratio of cell:Pt(II) = $1:6\times10^9$ for at least 30 min to allow metal ion-amine coordination. Subsequently, the cells were dehydrated through a graded ethanol series (10 min incubation each in 25%, 50%, 60%, 70%, 80%, 90%, 95%, and 100% ethanol), followed by hexamethyldisilazane treatment for 5 min, and drying in air [36,37].

Topographic and current images were acquired in contact mode using an Agilent 5500 AFM (Agilent Technologies, CA). The probes consist of Pt coated Si microlevers (ElectriContG, Budget Sensors, Bulgaria) with a spring constant of 0.2 N/m. Typical scanning rate was 1 Hz while force was kept at 20 nN. All the images were acquired with a pixel size of 512 × 512 except for images shown in Fig. 2 (c) and (d) and Fig. 4 (a) and (b) with a pixel size of 256 × 256. The scanner was enclosed in a small chamber to allow regulation of atmosphere and humidity. Once bias voltage was applied between the Au substrate and the conductive AFM tip, current as low as pA could be measured through a 10 V/nA transconductance amplifier. The quality and conductivity of Pt-coating were checked by imaging SAM regions before and after cellular imaging (see details in Section 3). Damage or contamination of Pt coating among AFM probes could easily be detected by a sudden drop of current and altering of the SAM's conductivity. In a typical experiment, 1- 4 hrs, little change in Pt-coating was detected.

3. RESULTS AND DISCUSSION

CAFM imaging of cells is illustrated schematically in Fig. 1 (a). Typically, three images were acquired simultaneously: topography, force, and current. Following the preparation protocols discussed in the previous section, cells were immobilized onto the FN covered region [38], while most FN molecules in the surrounding aldehyde-terminated SAM regions were washed away.

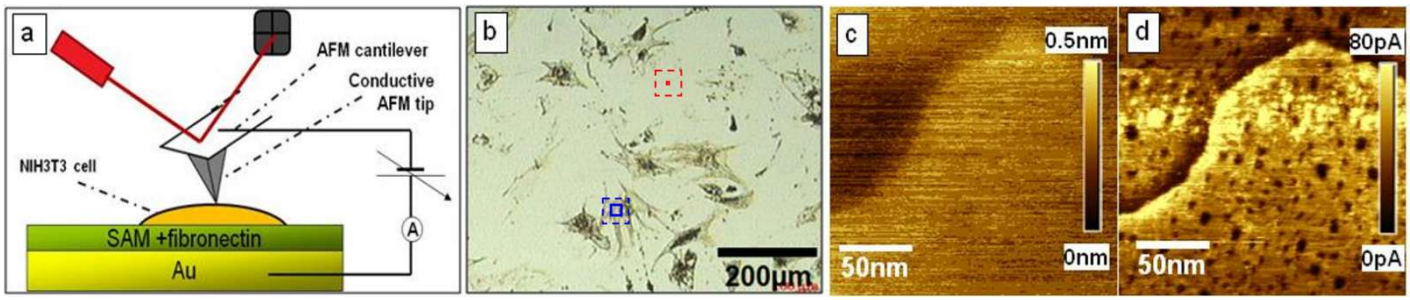

Figure 1. [a] Schematic diagram for imaging NIH3T3 cells by CAFM. [b] Bright-field optical image of the NIH 3T3 cells. CAFM topography [c] and current [d] images of a $CHO(CH_2)_{10}S$/Au(111) SAM under +1 V at ambient conditions at 1 Hz scan rate.

Understanding that the quality of CAFM probes could vary and some could be damaged or severely contaminated during shipping or handling at the apex, we tested and verified the quality of Pt-coating for AFM probes prior to imaging of cells. The test was performed *in situ* by imaging SAM regions (marked with a red dot in a red dashed bordered square in Fig. 1 (b). Under ambient conditions and with a bias of +1 V, the topography and current images are shown in Figs. 1(c) and 1(d), respectively. As shown in Fig. 1(c), one step, 0.2~0.3 nm tall, is visible in the AFM topography. This feature represents a SAM covered Au(111) single atomic step. In the current image, two features are clearly visible: the step and etch pits (2~10 nm in diameter). These features are characteristic of SAMs on Au(111) [39-41]. The etch pits are typically one Au(111) step deep, and covered by thioladsorbate [39,40]. In terms of the resistance, the etch pits and the surrounding areas should not differ as reviewed by our prior investigation using scanning tunneling microscopy.[31,42,43]

However, the apexes of Pt-coated AFM tips are10-20 nm, wider than the diameter of a typical pit, and as such the tips cannot reach the bottom of the pits. This results in a higher resistance of the tip-sample contact while scanning over a pit, which manifested in lower current contrast than the surrounding. The CAFM current in the closely packed domain regions measures 50-100 pA under +1 V bias, consistent with the known conductivity of thiol SAMs on gold [25,28,44-46]. In addition, the current signal increasing with the force was observed in CAFM studies of alkanethiol SAMs on Au[25] and alkylsiloxane SAMs on Si(111) surfaces [47]. These tests, collectively, ensured the quality of the conductive probes before and after cellular imaging.

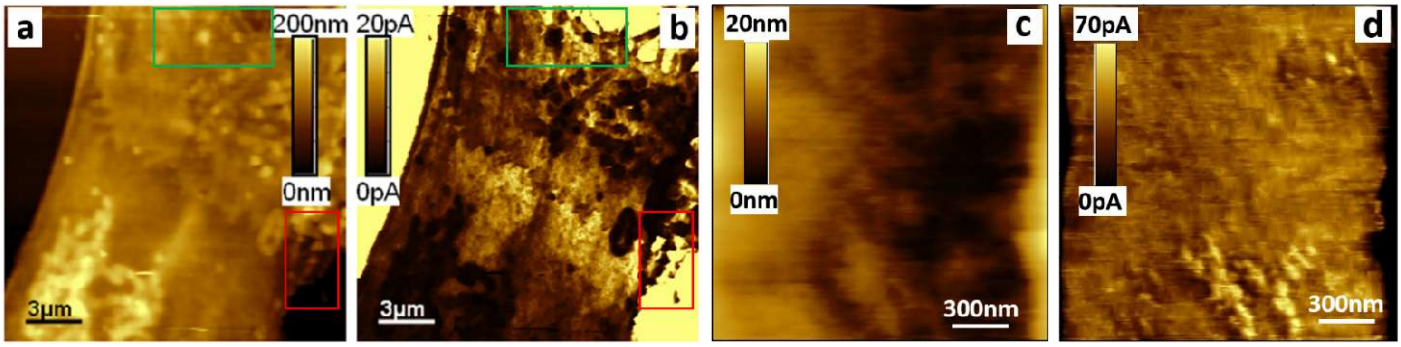

Figure 2. CAFM topography [a] and current [b] images of a filopodium region of a NIH 3T3 cell on a FN-functionalized surface in 100% humidity (scan area 20 µm × 20 µm).[c] and [d] are CAFM topography and current images, respectively, acquired over 2 µm × 2 µm. All the images were obtained with a bias of -10 V at 1 Hz scan rate.

Fig. 2 illustrates the typical contrast and resolution CAFM can reach under our configuration. Cell coverage on surfaces was deliberately kept low, as shown in Fig. 1(b), to allow selection and imaging of individual cells and intracellular regions. Cell spreading on the surface exhibits the characteristic polygon- or star-shaped morphologies (shown in Fig. 1(b)) known for NIH 3T3 cells with mature focal adhesion.[34] Zooming into a filopodium, as shown with a blue open square within a blue dashed bordered square in Fig. 1(b), the topography and simultaneous current images were acquired, shown in Figs. 2(a) and (b), respectively. The current signal acquired from the SAM surrounding reached the upper limit (1 nA) of the current sensor, resulting in the bright yellow contrast in Fig. 2(b). The current in the podium ranges 0-20 pA, thus exhibiting darker contrast in comparison to the surrounding SAMs. In the corresponding topography, the SAM is much lower in height, i.e. the dark regions in Fig. 2 (a). Figs. 2(a) and 2(b) confirm the clear boundaries between cellular region and SAM areas. From the topography in Fig. 2(a), many structural features within the podium are visible, such as dots. The corresponding current image in Fig. 2(b) reveals that most of them appear as darker contrast features than the nearby podium region, such as in the green frame. This observation is consistent with the anticipation that thicker materials yield lower current (or higher resistance). The boundaries in the current image for these structural features are sharper than in the topography image, therefore enabling accurate determination of their lateral dimensions. For the three bright dots shown in the green frame in Fig. 2(a), the corresponding lateral dimensions in Fig. 2(b) are 800 nm, 950 nm, and 1150 nm, respectively. These accurately determined fine features are consistent with microvilli present with fibroblast cells [38,48]. Smaller area scans allow us to see smaller features, as shown in Figs. 2(c) and 2(d). In Fig. 2 (d), bright features are visible, indicating resolution higher than 20 nm.

In the case of line features (typically along the main axis), the current images appear brighter, i.e., more conductive despite the taller topography, such as the line near the left edge and short lines inside the red frame in Fig. 2(a). This is consistent with the presence of F-actin in these regions, formed upon mature focal adhesion. The protein in the F-actin region exhibit favorable coordination with Pt(II) due to the high density of amine functionalities [49] which manifests into higher conductance. Some dot-features, as shown in the red frame, also show higher conductance, in contrast to the majority of the villi features. We are not clear what the structural basis for these features is, but could infer that these are likely protein rich domains that could coordinate with Pt(II).

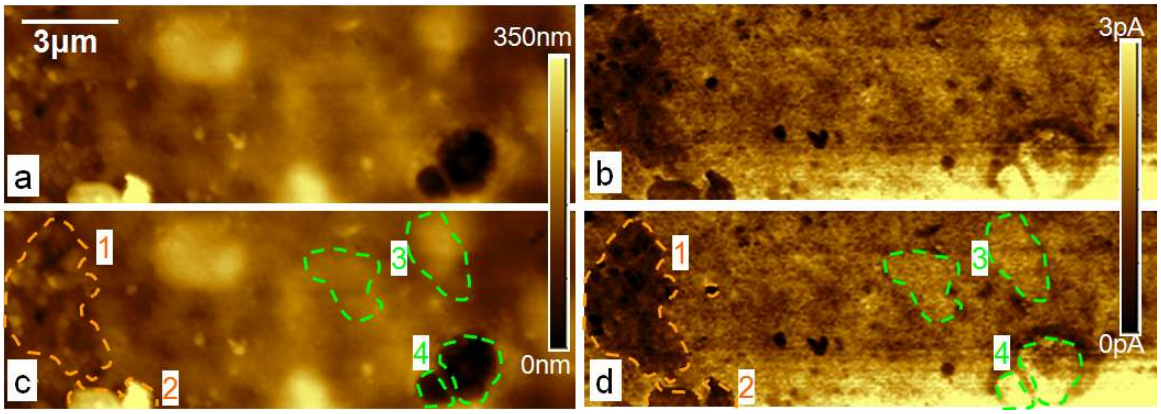

Figure 3. CAFM topography [a] and current [b] images of the central region of a Pt(II) stained NIH3T3 cell on FN-functionalized Au substrate imaged in 100% humid air with a bias of -10 V at 1 Hz scan rate. [c] and [d] correspond to images [a] and [b] respectively with features of interest being marked by orange and green contours and numbers. All the images are displayed with the same scale bar shown in [a].

Fig. 3 demonstrates that CAFM probes can reveal more than simple topography. In the case of homogeneous materials, the current should reflect inversely the height or thickness profile, i.e., the topographic height correlates to lower current contrast. For non-homogeneous materials, one would not expect the same correspondence. Since the intracellular distribution of Pt(II) follows the outcome of coordination chemistry, e.g., amine residues with metal ions, the conductivity is likely to be heterogeneous. This prediction is clearly shown in Fig. 3 (a)-(d). Region 1 (enclosed by an orange dash line) is 50~100 nm lower than the surrounding areas in the topography image, while in the current image, its current is around 1 pA lower compared to the surrounding areas.

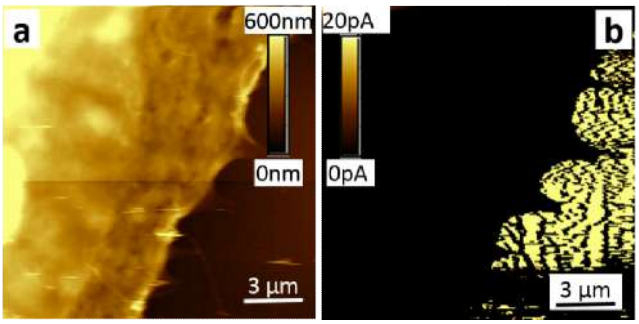

Figure 4. CAFM topography [a] and current [b] images of a podium region of an NIH 3T3 after soaking the sample in phosphate buffer solution (replacing Pt(II) with Na^+ ions). All the images were obtained with a bias of -10 V at 1 Hz scan rate.

Region 2 shows the inverse correlation between topography and current, 100 nm higher in topography and 1 pA lower in current image compared to its surrounding areas. Region 3 (enclosed by a green dash line) shows no significant contrast with the surrounding areas in both topography and current images, while region 4, seen as two craters of different size in topography, displays as two rings with lower current compared to the surrounding areas. The above observations demonstrate that the conductivity of the sample is not uniform. As the conductivity is mainly contributed by the metal ion doping, the contrast could indicate the locations where Pt(II) ions accumulate, such as protein rich regions.

In efforts to rationalize the observed conductivity, we imaged the same sample shown in Fig. 2 at a lower humidity, e.g. 40%, which exhibits little contrast in current images under the bias of -10 V. No current was measured at near 0% humidity in dry nitrogen atmosphere. These tests suggest that the presence of water is essential for the CAFM conductivity. Soaking the cells in phosphate buffer solution containing a high concentration of Na^+ resulted in reduction of Pt(II) ions within cells, and consequently led to the vanishing of the current signals (shown in Fig. 4 (a) and (b)). These experiments indicate that ion transport is not the primary contribution to CAFM current. The results are consistent with electron transport via Au surface (-10 V) to aqueous Pt(II), then to the conductive probe. Presently, we cannot further reveal the role of Pt(II), e.g., electron tunneling and/or redox reactions driven by the bias [50].

4. CONCLUSIONS

Nanometer resolution imaging of cells is attainable by most AFM instruments if cells are treated via transition metal ions. Using current sensing AFM and Pt(II) stained NIH3T3 cells, our work demonstrated that the cellular morphology and intracellular structural features, such as villi, podia, and fiber assemblies can be visualized. Finer membrane features (< 20 nm) are also observed. The high contrast in current images indicates where Pt(II) accumulated, e.g. protein rich regions. Our investigation pointsto electron transport as the likely mechanism in CAFM contrast. This approach enables researchers to quickly inspect cellular features using AFM without involving complex instrumentation, protocols, or sectioning of samples.

5. REFERENCES

[1] G. Binnig, C. F. Quate, C. Gerber, Atomic force microscope, *Phys. Rev. Lett. 56*, 930, **1986**.
[2] W. Haberle, J. K. H. Horber, G. Binnig, Force microscopy on living cells, *J. Vac. Sci. Technol. B,* 1210, **1991.**
[3] F. Ohnesorge, G. Binnig, True atomic resolution by atomic force microscopy through repulsive and attractive forces, *Science*, *260*, 1451, **1993**.
[4] J. P. Ruppersberg, J. K. H. Horber, C. Gerber, G. Binnig, maging of cell membraneous and cytoskeletal structures with a scanning tunneling microscope, *Febs Lett.*, *257*, 460, **1989**.
[5] Z. Deng, V. Lulevich, F.-T. Liu, G.-Y. J. Liu, Applications of Atomic Force Microscopy in Biophysical Chemistry of Cells, *Phys. Chem. B*, *114*, 5971, **2010**.
[6] J. E. Koehne, R. M. Stevens, T. Zink, Z. Deng, H. I. Chen, C. Weng, F. T. Liu, G. Y. Liu, Using carbon nanotube probes for high-resolution three-dimensional imaging of cells, *Ultramicroscopy*, *111*, 1155, **2011**.
[7] A. Engel, C.-A. Schoenenberger, D. J. Müller, High resolution imaging of native biological sample surfaces using scanning probe microscopy, *Curr. Opin. Struct. Biol.*, *7*, 279, **1997**.
[8] M. Radmacher, R. W. Tillmann, M. Fritz, H. E. Gaub, From molecules to cells: imaging soft samples with the atomic force microscope, *Science*, *257*, 1900, **1992**.
[9] A. I. Shevchuik, G. I. Frolenkov, D. Sanchez, P. S. James, N. Freedman, M. J. Lab, R. Jones, D. Klenerman, Y. E. Korchev, maging Proteins in Membranes of Living Cells by High-Resolution Scanning Ion Conductance Microscopy, *Angew. Chem. Int. Edit.*, *45*, 2212, **2006**.
[10] P. K. Hansma, J. P. Cleveland, M. Radmacher, D. A. Walters, P. E. Hillner, M. Bezanilla, M. V., D. Fritz, H. G. Hansma, Tapping mode atomic force microscopy in liquids , *Appl. Phys. Lett.*, *64*, 1738, **1994**.
[11] R. Lal, B. Drake, D. Blumberg, D. R. Saner, P. K. Hansma, S. C. Feinstein, Imaging real-time neurite outgrowth and cytoskeletal reorganization with an atomic force microscope, *Am. J. Physiol. Cell Physiol.*, *269*, C275, **1995**.
[12] R. Lal, H. Lin, A. P. Quist, Amyloid beta ion channel: 3D structure and relevance to amyloid channel paradigm, *Biochim. Biophys. Acta. Biomembranes*, *1768*, 1966, **2007**.
[13] K. Wadu-Mesthrige, N. A. Amro, J. C. Garno, S. Cruchon-Dupeyrat, G. Y. Liu, Contact Resonance Imaging - A Simple Approach to Improve the Resolution of AFM for Biological and Polymeric Materials, *Appl. Surf. Sci.*, *175*, 391, **2001**.
[14] H. J. Dai, J. H. Hafner, A. G. Rinzler, D. T. Colbert, R. E. Smalley, Nanotubes As Nanoprobes in Scanning Probe Microscopy, *Nature*, *384*, 147, **1996**.
[15] J. H. Hafner, C. L. Cheung, A. T. Woolley, C. M. Lieber, Structural and functional imaging with carbon nanotube AFM probes, *Prog. Biophys. Mol. Bio.*, *77*, 73, **2001**.
[16] H. Kim, K. Oikawa, N. Watanabe, M. Shigeno, Y. Shirakawabe, K. Yasuda, Identification of Size Differences of Gold Nanoparticles on Cell

Surface by Curvature Reconstruction Method Using Atomic Force Microscopy, *Jpn. J. Appl. Phys.*, *46*, L184, **2007**.
[17] J. Li, A. M. Cassell, H. J. Dai, Carbon nanotubes as AFM tips: Measuring DNA molecules at the liquid/solid interface, *Surf. Interface Anal.*, *28*, 8, **1999**.
[18] S. Amemiya, A. J. Bard, F.-R. F. Fan, M. V. Mirkin, P. R. Unwin, Scanning electrochemical microscopy, *Annu. Rev. Anal. Chem.*, *1*, 95, **2008**.
[19] J. Gorelik, Y. Zhang, A. I. Shevchuk, G. I. Frolenkov, D. Sánchez, M. J. Lab, I. Vodyanoy, C. R. W. Edwards, D. Klenerman, Y. E. Korchev, The use of scanning ion conductance microscopy to image A6 cells, *Mol. Cell. Endocrinol.*, *217*, 101, **2004**.
[20] R. Proksch, R. Lal, P. K. Hansma, D. Morse, G. Stucky, Imaging the internal and external pore structure of membranes in fluid: TappingMode scanning ion conductance microscopy, *Biophys. J.*, *71*, 2155, **1996**.
[21] Y. Takahashi, Y. Hirano, T. Yasukawa, H. Shiku, H. Yamada, T. Matsue, Topographic, electrochemical, and optical images captured using standing approach mode scanning electrochemical/optical microscopy, *Langmuir*, *22*, 10299, **2006**.
[22] R. T. Kurulugama, D. O. Wipf, S. A. Takacs, S. Pongmayteegul, P. A. Garris, J. E. Baur, Scanning electrochemical microscopy of model neurons: constant distance imaging, *Anal. Chem.*, *77*, 1111, **2005**.
[23] S. Amemiya, J. Guo, H. Xiong, D. Gross, Biological applications of scanning electrochemical microscopy: chemical imaging of single living cells and beyond, *Anal. Bioanal. Chem.*, *386*, 458, **2006**.
[24] S. Bergner, P. Vatsyayan, F.-M. Matysik, Recent advances in high resolution scanning electrochemical microscopy of living cells--a review, *Anal. Chim. Acta.*, *775*, 1, **2013**.
[25] Qi, Y., Ratera, I., Park, J. Y., Ashby, P. D., Quek, S. Y., Neaton, J. B., Salmeron, M. Mechanical and charge transport properties of alkanethiol self-assembled monolayers on a au(111) surface: the role of molecular tilt., *Langmuir*, *24*, 2219, **2008**.
[26] V. B. Engelkes, J. M. Beebe, C. D. *J.* Frisbie, Analysis of the causes of variance in resistance measurements on metal-molecule-metal junctions formed by conducting-probe atomic force microscopy, *Phys. Chem. B*, *109*, 16801, **2005**.
[27] D. C. Coffey, O. G. Reid, D. B. Rodovsky, G. P. Bartholomew, D. S. Ginger, Mapping Local Photocurrents in Polymer/Fullerene Solar Cells with Photoconductive Atomic Force Microscopy, *Nano Lett.*, *7*, 738, **2007**.
[28] J. Y. Park, Y. Qi, I., Ratera, M. Salmeron, Noncontact to contact tunneling microscopy in self-assembled monolayers of alkylthiols on gold, *J. Chem. Phys.*, *128*, 234701, **2008**.
[29] P. E. Laibinis, G. M. Whitesides, D. L. Allara, Y. T. Tao, A. N. Parikh, R. G. Nuzzo, Comparison of the structures and wetting properties of self-assembled monolayers of n-alkanethiols on the coinage metal surfaces, copper, silver, and gold, *J. Am. Chem. Soc.*, *113*, 7152, **1991**.
[30] J. C. Love, L. A., Estroff, J. K. Kriebel, R. G. Nuzzo, G. M. Whitesides, Self-assembled monolayers of thiolates on metals as a form of nanotechnology, *Chem. Rev.*, *105*, 1103, **2005**.
[31] A. Riposan, Y. Li, Y. H. Tan, G. Galli, G.-Y. Liu, Structural Characterization of Aldehyde–Terminated Self-Assembled Monolayers, *J. Phys. Chem. A*, *111*, 12727, **2007**.
[32] D. Bu, T. J. Mullen, G.-Y. Liu, Regulation of local structure and composition of binary disulfide and thiol self-assembled monolayers using nanografting, *ACS Nano*, *4*, 6863, **2010**.
[33] A. Riposan, Y. Li, Y. H. Tan, G. Galli, G.-Y.Liu, Structural Characterization of Aldehyde–Terminated Self-Assembled Monolayers, *J. Phys. Chem. A*, *111*, 12727, **2007**.
[34] L. Shi, J.-R. Li, Y.-P. Shih, S. Lo, G.-Y. Liu, Nanogratings of Fibronectin Provide an Effective Biochemical Cue for Regulating Focal Adhesion and Cellular Structure, *Nano Res.*, *5*, 565, **2012**.
[35] G. Y. Liu, N. A. Amro, Positioning protein molecules on surfaces: A nanoengineering approach to supramolecular chemistry, *P. Natl. Acad. Sci. USA*, *99*, 5165, **2002**.
[36] J. L. Nation, A new method using hexamethyldisilazane for preparation of soft insect tissues for scanning electron microscopy, *Stain Technol.*, *58*, 347, **1983**.
[37] J. Laterra, J. E. Silbert, L. A. Culp, Cell surface heparan sulfate mediates some adhesive responses to glycosaminoglycan-binding matrices, including fibronectin, *J. Cell Biol.*, *96*, 112, **1983**.
[38] G. Fuhr, E. Richter, H. Zimmermann, H. Hitzler, H. Niehus, R. Hagedorn, Cell traces--footprints of individual cells during locomotion and adhesion, *Biol. Chem.*, *379*, 1161, **1998**.
[39] G. E. Poirier, Mechanism of Formation of Au Vacancy Islands in Alkanethiol Monolayers on Au(111), *Langmuir*, *13*, 2019, **1997**.
[40] G. E. Poirier, Characterization of Organosulfur Molecular Monolayers on Au(111) using Scanning Tunneling Microscopy, *Chem. Rev.*, *97*, 1117, **1997**.
[41] D. Scaini, M. Castronovo, L. Casalis, G. Scoles, Electron transfer mediating properties of hydrocarbons as a function of chain length: a differential scanning conductive tip atomic force microscopy investigation, *ACS Nano*, *2*, 507, **2008**.
[42] G. Yang, G.-Y. Liu, New Insights for Self-Assembled Monolayers of Organothiols on Au(111) Revealed by Scanning Tunneling Microscopy, *J. Phys. Chem. B*, *107*, 8746, **2003**.
[43] Y. Qian, G. Yang, J. Yu, T. A. Jung, G.-Y. Liu, Structures of Annealed Decanethiol Self-Assembled Monolayers on Au(111): An Ultrahigh Vacuum Scanning Tunneling Microscopy Study, *Langmuir*, *19*, 6056, **2003**.
[44] D. J. Wold, R. Haag, M. A. Rampi, C. D. Frisbie, Distance Dependence of Electron Tunneling through Self-Assembled Monolayers Measured by Conducting Probe Atomic Force Microscopy: Unsaturated versus Saturated Molecular Junctions, *J. Phys. Chem. B*, *106*, 2813, **2002**.
[45] S. E. Fritz, S. Mohapatra, B. T. Holmes, A. M. Anderson, C. F. Prendergast, C. D. Frisbie, M. D. Ward, M. F. Toney, Thin film transistors based on alkylphenyl quaterthiophenes: Structure and electrical transport properties, *Chem. Mater.*, *19*, 1355, **2007**.
[46] L. S. C. Pingree, O. G. Reid, D. S. Ginger, *Adv. Mater*, Electrical Scanning Probe Microscopy on Active Organic Electronic Devices, *21*, 19, **2009**.
[47] J. Y. Park, Y. Qi, P. D. Ashby, B. L. M. Hendriksen, M. Salmeron, Electrical transport and mechanical properties of alkylsilane self-assembled monolayers on silicon surfaces probed by atomic force microscopy, *J. Chem. Phys.*, *130*, 114705, **2009**.
[48] H.-A. Pan, Y.-C. Hung, C.-W. Su, S.-M. Tai, C.-H. Chen, F.-H. Ko, G.S. Huang, Control of growth and inflammatory response of macrophages and foam cells with nanotopography, *Nanoscale Res. Lett.*, *4*, 903, **2009**.
[49] C. J. Fleming, N.-N. Yin, S. L. Riechers, G. Chu, G.-Y. Liu, High-resolution imaging of the intramolecular structure of indomethacin-carrying dendrimers by scanning tunneling microscopy., *ACS Nano*, *5*, 1685, **2011**.
[50] C. J. Fleming, Y. X. Liu, Z. Deng, G.-Y. Liu, Deformation and Hyperfine Structures of Dendrimers Investigated by Scanning Tunneling Microscopy, *J. Phys. Chem. A*, *113*, 4168, **2009**.

6. ACKNOWLEDGEMENTS

The authors gratefully acknowledge support from the National Science Foundation (NSF) and National Institutes of Health (1R21CA176850-01). AK and MS were supported by the Director, Office of Science, Office of Basic Energy Sciences, Chemical Sciences, Geosciences, and Biosciences Division, under the Department of Energy Contract No. DE-AC02-05CH11231. The imaging was performed at the Molecular Foundry of the LBNL, a user facility of the DOE Office of Science. We also thank Dr. F. Martin at LBNL and Dr. J Li at UCD for their technical assistance, and Mr. L. Swartz, and Mr. Y. Liu for helpful discussions.